Far-from-equilibrium growth of magnetic thin films with Blume-Capel impurities

Karina I. Mazzitello,[1] Julián Candia,[2,3,*] and Ezequiel V. Albano[2,4]
[1]*Departamento de Física (UNMdP), Mar del Plata, Argentina*
[2]*Instituto de Física de Líquidos y Sistemas Biológicos (CONICET, UNLP), La Plata, Argentina*
[3]*Department of Physics, University of Maryland, College Park, Maryland 20742, USA*
[4]*Departamento de Física (UNLP), La Plata, Argentina*
(Received 11 December 2014; published 16 April 2015)

We investigate the irreversible growth of $(2+1)$-dimensional magnetic thin films. The spin variable can adopt three states ($s_i = \pm 1,0$), and the system is in contact with a thermal bath of temperature T. The deposition process depends on the change of the configuration energy, which, by analogy to the Blume-Capel Hamiltonian in equilibrium systems, depends on Ising-like couplings between neighboring spins (J) and has a crystal field (D) term that controls the density of nonmagnetic impurities ($s_i = 0$). Once deposited, particles are not allowed to flip, diffuse, or detach. By means of extensive Monte Carlo simulations, we obtain the phase diagram in the crystal field vs temperature parameter space. We show clear evidence of the existence of a tricritical point located at $D_t/J = 1.145(10)$ and $k_B T_t/J = 0.425(10)$, which separates a first-order transition curve at lower temperatures from a critical second-order transition curve at higher temperatures, in analogy with the previously studied equilibrium Blume-Capel model. Furthermore, we show that, along the second-order transition curve, the critical behavior of the irreversible growth model can be described by means of the critical exponents of the two-dimensional Ising model under equilibrium conditions. Therefore, our findings provide a link between well-known theoretical equilibrium models and nonequilibrium growth processes that are of great interest for many experimental applications, as well as a paradigmatic topic of study in current statistical physics.

DOI: 10.1103/PhysRevE.91.042118 PACS number(s): 05.70.Fh, 05.10.Ln, 64.60.an, 75.70.−i

I. INTRODUCTION

Nowadays, thin-film technology is playing an outstanding role in several areas of basic and applied research, from the manufacture of optics (reflective and antireflective coatings, self-cleaning glasses, etc.) to electronics (layers of insulators, semiconductors, and conductors from integrated circuits) and packaging (e.g., aluminium-coated PET films). Nanoscale deposition techniques such as sputtering and molecular beam epitaxy, which allow a single layer of atoms to be deposited at a time and therefore grant significant control over the thin-film growth process, have stimulated the research and development of novel materials [1–8].

In particular, some of these research efforts have focused on magnetic thin films such as the $L1_0$ phase of Fe/Pt, which is currently the leading candidate material for ultra-high-density heat-assisted magnetic recording (HAMR) and bit-patterned magnetic recording (BPMR) media [9–11]. It is well known that the properties of such magnetic thin films may depend strongly on the presence of impurities. Moreover, even nonmagnetic materials such as CaB_6 [12–14] and the semiconducting oxide TiO_2 [15] may exhibit room-temperature ferromagnetism, an intriguing phenomenon possibly driven by the presence of magnetic and/or nonmagnetic impurities. This kind of phenomena has attracted a great deal of attention in recent years and has emerged as one important branch in condensed matter physics and materials science [16–20].

On the theoretical side, a well-known equilibrium magnetic system that includes the effect of impurities is the so-called Blume-Capel model, which has been extensively studied using mean-field theory [21], real-space renormalization group calculations [22], ϵ-expansion renormalization groups [23], Monte Carlo renormalization-group analysis [24], high- and low-temperature series calculations [25], Monte Carlo simulations [26], and finite-size scaling and conformal invariance [27]. Indeed, the Blume-Capel model has attracted considerable attention due to its interesting physical behavior and its broad applications in the theory of fluids and magnetism (see, e.g., Refs. [28,29]). Some recent theoretical studies of Blume-Capel systems include short-time dynamics [30] and Wang-Landau Monte Carlo simulations [31], mixed spin ferromagnets on the Bethe lattice [32], dynamic phase transitions in oscillating external fields [33], bond randomness [34], random crystal effects [35], and wetting transitions in confined geometries [36,37], among others.

The Blume-Capel (BC) Hamiltonian, which considers a three-state spin system ($s_i = \pm 1,0$), has an Ising-like term proportional to the coupling constant J that takes into account the interaction between nearest-neighbor spins, as well as a term proportional to the crystal field D that controls the density of nonmagnetic impurities (or vacancies, depending on the interpretation of the model). The phase diagram of the equilibrium BC model in two dimensions and in the absence of magnetic fields is very well known. The model exhibits ordered ferromagnetic and disordered paramagnetic phases separated by a transition line, which changes from a continuous phase transition (that belongs to the Ising universality class) to a first-order transition at the tricritical point. In fact, in the $D \to -\infty$ limit, impurities are excluded and the BC model reduces to the classical two-state Ising model, while for sufficiently large crystal fields, the transition becomes first order and separates the impurity-dominated phase from the ordered phase dominated by up or down spins. Thus, these three coexisting phases give rise to a tricritical point located

*Present and permanent address: Center for Human Immunology, National Institutes of Health, Bethesda, MD, USA.

at $k_B T_t/J = 0.609(5)$ and $D_t/J = 1.965(5)$, valid for two dimensions, where k_B and J are the Boltzmann constant and the spin-spin coupling, respectively [30]. This description of the phase diagram of BC model holds for spin-1 model, while for higher values of the spin the corresponding phase diagrams are richer.

In the context of current efforts focused on the effect of impurities on far-from-equilibrium deposition processes (see, e.g., Refs. [38–40]), the aim of this work is to investigate the irreversible growth of magnetic thin films with BC impurities in $(2+1)$-dimensional strip geometries. Magnetic films growing under far-from-equilibrium conditions are investigated by using the magnetic Eden model (MEM) [41,42], an extension of the classical Eden model [43] in which particles have an additional degree of freedom (the spin). Earlier studies have shown that films growing in $(d+1)$-dimensional strip geometries in an homogeneous thermal bath are noncritical for $d = 1$, while they undergo order-disorder phase transitions that take place at $k_B T_c^{\rm hom}/J = 0.69(1)$ for $d = 2$ and spin-1/2 [42].

By means of extensive Monte Carlo simulations, we explore the behavior of thin-film growth in the crystal field *versus* temperature parameter space and obtain the corresponding phase diagram. In analogy with Ising-like equilibrium systems, we show clear evidence of the existence of a tricritical point located at $D_t/J = 1.145(10)$ and $k_B T_t/J = 0.425(10)$, which separates a first-order transition curve at lower temperatures from a critical second-order transition curve at higher temperatures. Since the MEM growth process is irreversible (i.e., newly deposited particles are not allowed to flip and thermalize once they are added to the growing cluster), the observed behavior resembling equilibrium spin models is intriguing and nontrivial. Therefore, we believe that our findings provide a link between the well-studied theoretical equilibrium models and more realistic nonequilibrium growth processes that are found in many experimental applications.

The rest of the paper is laid out as follows. In Sec. II, we introduce the model and describe the Monte Carlo algorithm used to simulate MEM thin films with Blume-Capel impurities. In Sec. III, we present our results and a discussion. Finally, Sec. IV consists of concluding remarks.

II. MODEL AND MONTE CARLO SIMULATION METHOD

The magnetic Eden model with Blume-Capel interactions (MEM-BC) in $(2+1)$ dimensions is studied in the square lattice by using a rectangular geometry $L_x \times L_y \times L_z$, where $L_z \gg L_x = L_y \equiv L$ is the growth direction. The location of each spin on the lattice is specified through its coordinates (x,y,z) $(1 \leqslant x,y \leqslant L,\ 1 \leqslant z \leqslant L_z)$. The starting seed for the growing cluster is a plane of $L \times L$ parallel-oriented spins placed at $z = 1$, and cluster growth takes place along the positive longitudinal direction (i.e., $z \geqslant 2$). Periodic boundary conditions are considered along both the x and the y axis.

Clusters are grown by selectively adding spins ($S_{xyz} = 0, \pm 1$) to perimeter sites, which are defined as the nearest-neighbor (NN) empty sites of the already occupied ones. The $S = 0$ particles can be considered nonmagnetic impurities or, alternatively, they can be interpreted as vacancies, while the $S = \pm 1$ states can be interpreted as up/down magnetic spins or as binary mixtures of two different particle species. We will use a magnetic terminology throughout. Considering a ferromagnetic interaction of strength $J > 0$ between NN spins and a crystal field D to control the density of impurities, the

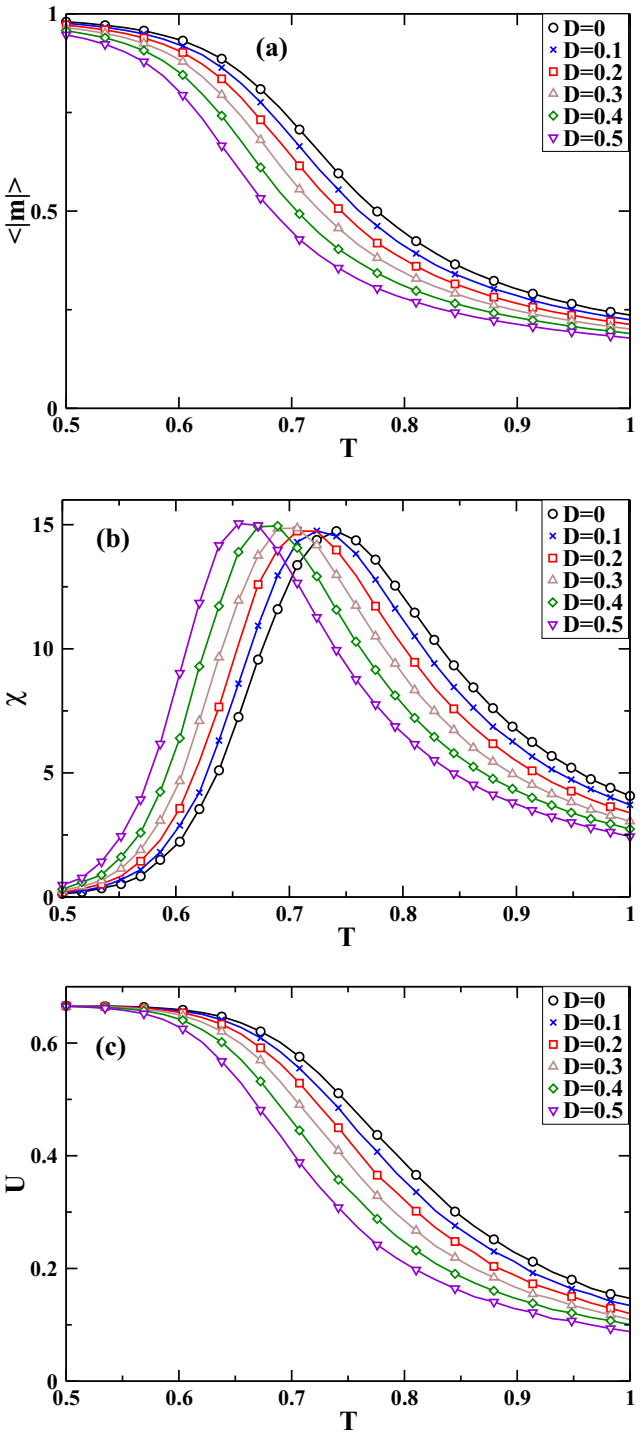

FIG. 1. (Color online) (a) Average absolute value of the magnetization $\langle |m| \rangle$, (b) susceptibility χ, and (c) Binder cumulant U versus temperature, corresponding to different choices of the crystal field D, as indicated. Data obtained by using samples of linear size $L = 12$. The temperature and the crystal field D are measured in units of J/k_B and J, respectively.

energy E of a given configuration of particles is given by

$$E = -\frac{J}{2} \sum_{\langle xyz, x'y'z' \rangle} S_{xyz} S_{x'y'z'} + D \sum_{xyz} S_{xyz}^2, \qquad (1)$$

where the summations are taken over occupied NN sites. The probability for a perimeter site to be occupied by a particle is proportional to the Boltzmann factor $\exp(-\Delta E/k_B T)$, where ΔE is the change of energy involved in the addition of the particle and T is the temperature of the thermal bath.

At each step, all perimeter sites have to be considered and the probabilities of adding a new particle (with spin up, down, or null) to each site must be evaluated. Using the Monte Carlo simulation method, after all probabilities are computed and normalized, the growth site and the value for the new spin are both simultaneously determined by means of one pseudorandom number. Notice that the MEM's growth rules require updating the probabilities at each time step and lead to very slow algorithms compared with analogous equilibrium spin models. Also, let us point out again that, although Eq. (1) resembles the Blume-Capel Hamiltonian, the MEM-BC is a nonequilibrium model in which new particles are continuously added, while older spins remain frozen and are not allowed to flip, detach, or diffuse.

Since the observables of interest (e.g., the mean magnetization in transverse x-y planes and its higher moments) require the growth of samples with a large number of transverse planes of size $L \times L$, clusters having up to 10^9 spins have typically been grown for lattice sizes in the range $12 \leqslant L \leqslant 128$. It should be mentioned that the advancing growth front leaves voids behind, which are incorporated to the bulk of the sample during some transient period. However, since the boundaries of these voids are also perimeter sites, they ultimately become filled in at some point during the growth process. Hence, far behind the active growth interface, the system is compact and frozen. The observables of interest can thus be measured on defect-free transverse planes.

Notice that the growth of magnetic Eden aggregates in $(2+1)$-strip geometries is characterized by an initial transient length $\ell_T \sim L^2$ (measured along the growth direction, i.e., the z axis) followed by a nonequilibrium stationary state that is independent of the initial configuration [42]. By disregarding the transient region, all results reported in this paper are obtained under stationary conditions. Since the strips are effectively semi-infinite and the substrate length along the growth direction plays no role, the only characteristic length is the transverse linear size L. As order parameter, we measured the absolute magnetization, which is given by

$$\langle |m| \rangle = \left\langle \left| \frac{1}{L^2} \sum_{xy} S_{x,y,z} \right| \right\rangle, \qquad (2)$$

where $\langle \ldots \rangle$ indicates the thermal average taken over parallel transverse planes with $z > \ell_T$. We also computed the

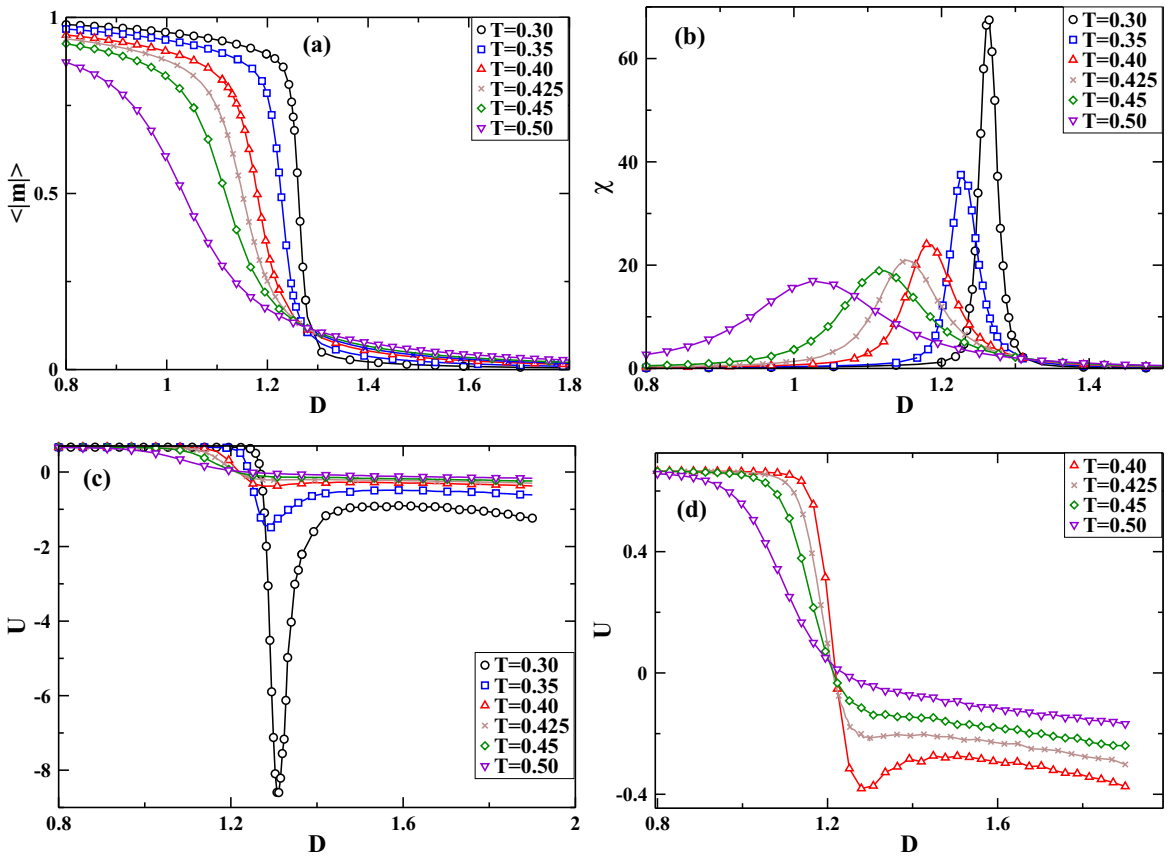

FIG. 2. (Color online) (a) Average absolute value of the magnetization $\langle |m| \rangle$, (b) susceptibility χ, and (c) Binder cumulant U versus crystal field D. (d) shows in detail the behavior of the cumulant within the relevant temperature interval, namely $0.40 \leqslant k_B T/J \leqslant 0.50$. Data obtained for different choices of the temperature T and by using samples of linear size $L = 12$.

fluctuations of the order parameter, which play the role of the susceptibility χ, i.e.,

$$\chi = \frac{L^2}{T}(\langle m^2\rangle - \langle m\rangle^2), \tag{3}$$

as well as the Binder cumulant U defined as

$$U = 1 - \langle m^4\rangle/[3\langle m^2\rangle^2]. \tag{4}$$

III. RESULTS AND DISCUSSION

In order to gain some insight on the growth process of the MEM-BC model, Figs. 1(a)–1(c) show plots of the order parameter, susceptibility, and Binder cumulant as functions of the temperature for different values of the crystal field. Figure 1(a) carries the signature of continuous transitions between an ordered state of high magnetization and a disordered state where the magnetization tends to vanish (except for finite-size effects that prevent the absolute magnetization from becoming strictly zero as $T \to \infty$). This scenario is further confirmed by the peaks observed in the susceptibility, as well as by the smoothly decreasing behavior of the Binder cumulant. Although finite systems can only provide information of effective, size-dependent pseudocritical temperatures, e.g., as given by the location of the peaks of the susceptibility, or by the transitions evidenced by the magnetization and cumulant profiles, Figs. 1(a)–1(c) show evidence that these effective pseudocritical temperatures decrease as the crystal field increases, as in the case of the equilibrium BC counterpart [21,36]. In all figures, the errors are of symbol size or less.

Similarly, Figs. 2(a)–2(c) show plots of the order parameter, susceptibility, and Binder cumulant versus the crystal field D, respectively. These measurements, performed at different temperatures, show the magnetization crossover from a smooth order-disorder effective transition observed at higher temperatures ($k_BT/J \geqslant 0.45$) to a much sharper drop at lower temperatures ($k_BT/J < 0.40$). This behavior is consistent with the shape of the peaks of the susceptibility that become narrower when the temperature is decreased [cf. Fig. 1(b) where the shape of the peaks of χ remains almost unchanged regardless of the values of D]. Indeed, these abrupt drops of $\langle|m|\rangle$ and sharp peaks of χ, as well as the local minima of U observed in a narrow interval of the crystal field, are all indicative of first-order effective transitions, as also observed in the standard BC model under equilibrium conditions. The onset of hallmark first-order behavior can clearly be observed in Figs. 2(c)–2(d), where one observes that the characteristic smooth, monotonically decreasing second-order behavior at high temperatures develops a local minimum at the effective first-order transition for lower temperatures.

The scenario emerging from the analysis of Figs. 1 and 2 is consistent with the effective D vs T phase diagram shown in Fig. 3. This phase diagram exhibits a line of continuous order-disorder transitions between ferromagnetic and paramagnetic phases in the high-T, low-D region, characterized by low impurity densities. On the other hand, the low-T, high-D region exhibits a line of sharp transitions with first-order behavior between the ferromagnetic state and a phase dominated by nonmagnetic impurities. The first- and second-order

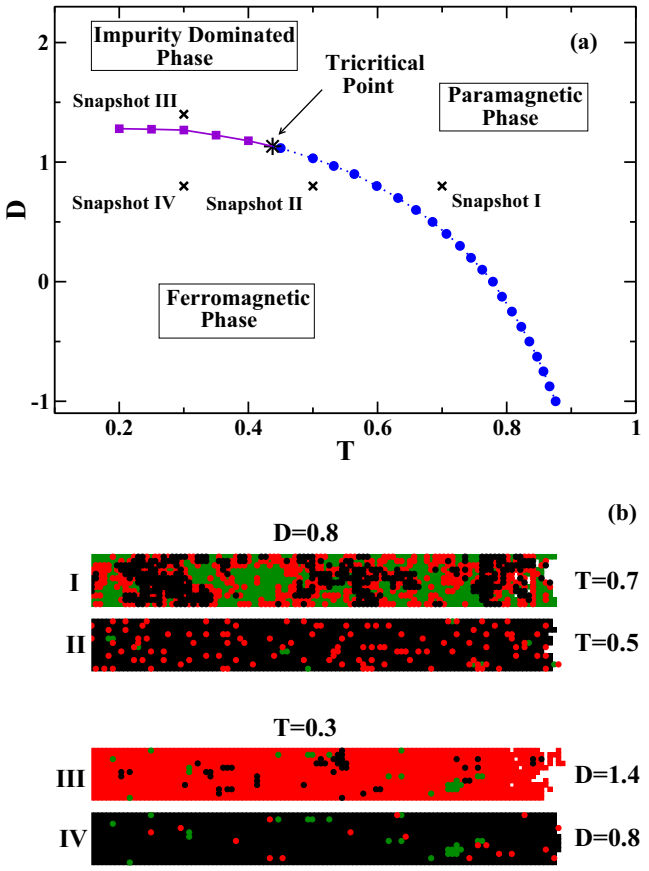

FIG. 3. (Color online) (a) Effective phase diagram of the MEM-BC model obtained by using samples of linear size $L = 12$. Circles and squares indicate lines of second- and first-order effective transitions, respectively, which meet each other at the effective tricritical point marked with a star. (b) Characteristic snapshots representing growth regimes dominated by different mixtures of impurities in red (gray), up spins in black and down spins in green (light gray).

transition lines meet each other at the effective tricritical point located at $k_BT_{\rm tri}^{\rm eff}(L = 12)/J \simeq 0.425(10)$, $D_{\rm tri}^{\rm eff}(L = 12)/J \simeq 1.145(10)$, also indicated in Fig. 3(a). Typical snapshot configurations representative of different states are shown in Fig. 3(b). Snapshots I, II, and IV were obtained for $D = 0.8$ and different temperatures, decreasing from $T = 0.7$ to $T = 0.3$. This trajectory in phase space runs across a second-order transition, from a disordered paramagnetic phase (Snapshot I) to highly ordered ferromagnetic states (Snapshots II and IV). On the other hand, Snapshots III and IV correspond to $T = 0.3$ and different values of the crystal field across a first-order transition, as indicated. The concentrations of up and down spins (black and green, respectively) and impurities (red) gradually change across the second-order transition ($I \to II$), while they sharply change across the first-order transition ($III \to IV$), in which a phase dominated by impurities (III) evolves into a phase dominated by up or down spins (IV). These variations are shown in Fig. 4. For D fixed, a wide scan of T is needed to observe variations of the probability distributions of the magnetization and impurities across the second-order transition line [Figs. 4(a)–4(b)]. In contrast, for T fixed at a temperature below the tricritical

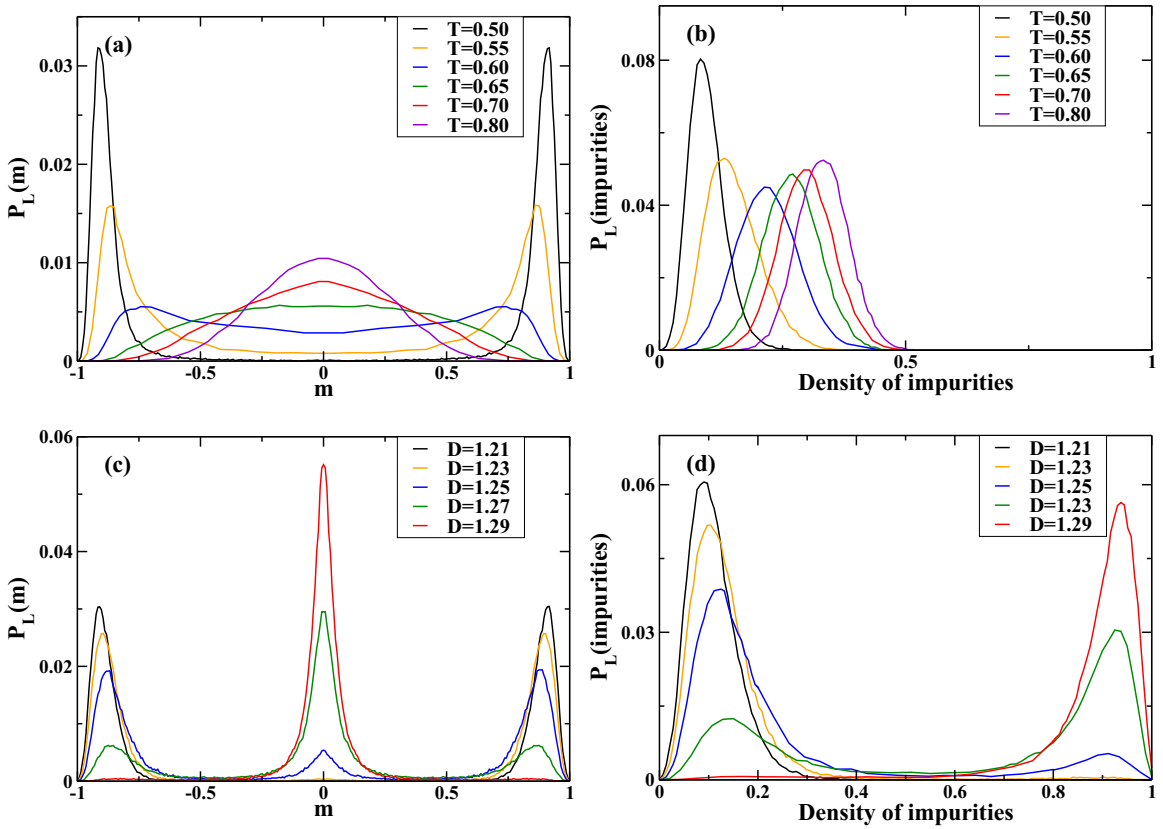

FIG. 4. (Color online) Probability distributions of the magnetization $P_L(m)$ [(a), (c)] and the density of impurities P_L(impurities) for different values of T and D. (a)–(b) For $D/J = 0.8$, the effective second-order transition occurs at $k_B T_c^{\rm eff}/J = 0.60(1)$. (c)–(d) For $k_B T/J = 0.3$, the effective first-order transition occurs at $D_c^{\rm eff}/J = 1.27(1)$. Data obtained by using samples of linear size $L = 12$.

point, a narrow scan of D performed close to the first-order transition line is enough to observe large variations of the probability distributions [Figs. 4(c)–4(d)]. Similarly, narrow scans of T (for D fixed at a crystal field above the tricritical point) close to the first-order transition lead to large variations of the probability distributions (not shown here for the sake of space).

Figure 5(a) confirms that, indeed, for very large values of D the system is dominated by impurities. Together with Figs. 5(b) and 5(c), which display fluctuations in the density of impurities and the corresponding Binder cumulant, respectively, these panels show that the behavior of the impurity density is consistent with sharp, first-order transitions at low temperatures and smooth, continuous second-order transitions at high temperatures.

In order to identify true phase transitions, however, Monte Carlo simulations must be performed on samples of different size that enable the subsequent application of finite-size scaling theory, which allows us to extrapolate results from finite samples to the thermodynamic ($L \to \infty$) limit. For this purpose, Figs. 6(a), 6(b), and 6(c) show plots of the average absolute magnetization $\langle |m| \rangle$, the susceptibility χ, and the Binder cumulant U versus the temperature T for $D = 0$ and samples of different size.

By analogy to the case of second-order transitions under equilibrium conditions [44,45] and according to the experience gained by studying the critical behavior of the far-from-equilibrium growth of MEM films [42], we assume that the characteristic length of MEM-BC clusters is given by a diverging correlation length (ξ) that behaves as

$$\xi \propto (T - T_c)^{-\nu}, \tag{5}$$

where T_c is the critical temperature and ν is the correlation length critical exponent. When ξ is of the order of the sample size, $\xi \simeq L$, finite-size effects are observed, such as the rounding and shifting of the peaks of the susceptibility shown in Fig. 6(b). From Eq. (5), it follows that

$$T_c^{\rm eff}(L) = T_c(L = \infty) + \text{const}\, L^{-1/\nu}, \tag{6}$$

where $T_c^{\rm eff}(L)$ is the size-dependent effective critical temperature, which can be identified, for instance, by the location of the peak of the susceptibility, while $T_c(L = \infty)$ is the true critical temperature corresponding to the thermodynamic limit. The inset of Fig. 6(b) shows the extrapolation performed by means of Eq. (6), where finite-size, effective critical temperatures are defined by the location of the peaks of χ, i.e., $T_c^{\rm eff}(L) \equiv T_{\chi_{\rm max}}$. Here, we assume $\nu = 1$ as in the cases of both the two-dimensional (2D) BC model under equilibrium conditions, as well as the MEM in $(2 + 1)$ dimensions [42]. More evidence for $\nu = 1$ as an appropriate value for the MEM-BC correlation length critical exponent is provided below via finite-size scaling data collapse (see Fig. 7 and discussion below). From the best fit of the data, we obtained $k_B T_c/J = 0.647(15)$ for $D = 0$.

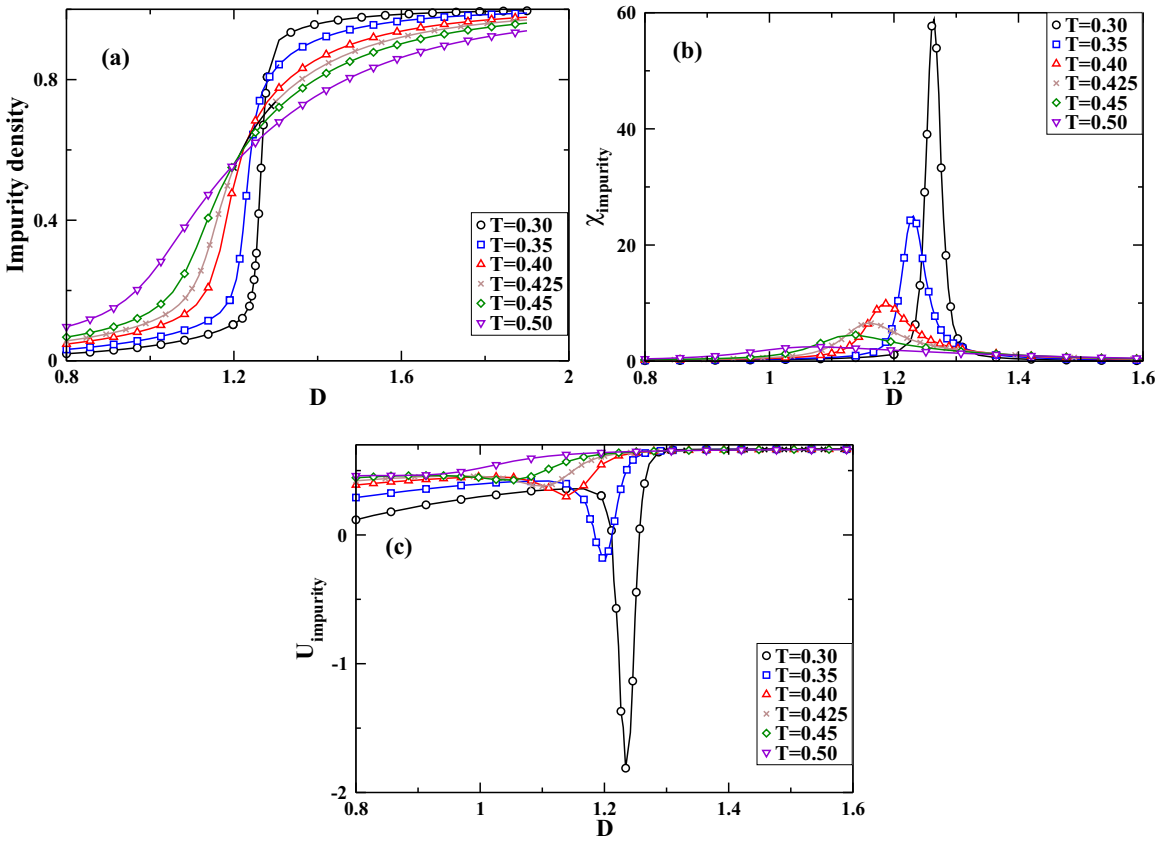

FIG. 5. (Color online) (a) Average density of impurities, (b) fluctuations in the impurity density (i.e., susceptibility for impurities, χ_{impurity}), and (c) Binder cumulant of impurities, U_{impurity}, as functions of the crystal field, D. Data obtained for different values of the temperature T and by using samples of linear size $L = 12$.

Finite-size scaling theory for critical phenomena, originally developed for systems under equilibrium [44,45] but later also successfully applied to far-from-equilibrium systems [46] and to irreversible phase transitions [47], establishes that the order parameter scales as

$$\langle |m| \rangle \propto L^{-\beta/\nu} m^*\{|T - T_c| L^{1/\nu}\}, \tag{7}$$

where β is the order parameter critical exponent and m^* is a suitable scaling function. Figure 7(a) shows that the data from Fig. 6(a) can be fully collapsed by finite-size scaling [Eq. (7)] by taking $\nu = 1$ and $\beta = 1/8$, i.e., the critical exponents of the 2D BC model in equilibrium, which also hold true, within error bars, for the far-from equilibrium MEM in $(2 + 1)$ dimensions [42]. On the other hand, the scaling behavior of the Binder cumulant, given by

$$U \propto U^*\{|T - T_c| L^{1/\nu}\}\,, \tag{8}$$

where U^* is a suitable scaling function, is also nicely satisfied by the collapse of the data from Fig. 6(c), as shown in Fig. 7(b).

Summing up, our results for the second-order transition of the MEM-BC growth model in $(2 + 1)$ dimensions obtained for $D = 0$, as well a set of results analyzed with a similar procedure but performed for different values of the crystal field (not shown here for the sake of space), confirms that the transition belongs to the same universality class than the 2D Ising model under equilibrium conditions. Additionally, in previous papers [42] we have shown that the MEM in $(2 + 1)$ dimensions, which corresponds to the MEM-BC model for $D = -\infty$, also belongs to the same universality class. Therefore, all results are consistent with the presence of a line of second-order transitions in the Ising universality class, as in the case of the 2D BC model under equilibrium [48]. Indeed, this finding supports early conjectures [49,50] pointing out that the universality class of growth models in $(d + 1)$ dimensions under far-from-equilibrium conditions is the same than that of their corresponding equilibrium counterparts but in d dimensions. In particular, here we provide robust evidence for the case $d = 2$, while, of course, $d = 1$ models are not critical in either case (equilibrium and far from it).

Besides this analysis of continuous second-order transitions, we have performed a systematic study of the occurrence of first-order transitions, as, e.g., shown in Figs. 2 and 5 (as well as in sets of results not shown here for the sake of space) in order to draw the complete phase diagram of the MEM-BC growth model shown in Fig. 8. We observe that lines of second- and first-order effective transitions meet each other at an effective tricritical point whose position is essentially independent of the lattice size, as displayed in greater detail in the inset to Fig. 8. In order to understand this observation, we recall that the effective critical temperature decreases with sample size following Eq. (6), while on the other hand, the coexistence temperatures associated to first-order transitions increase with the size, for D fixed. Close to those transitions,

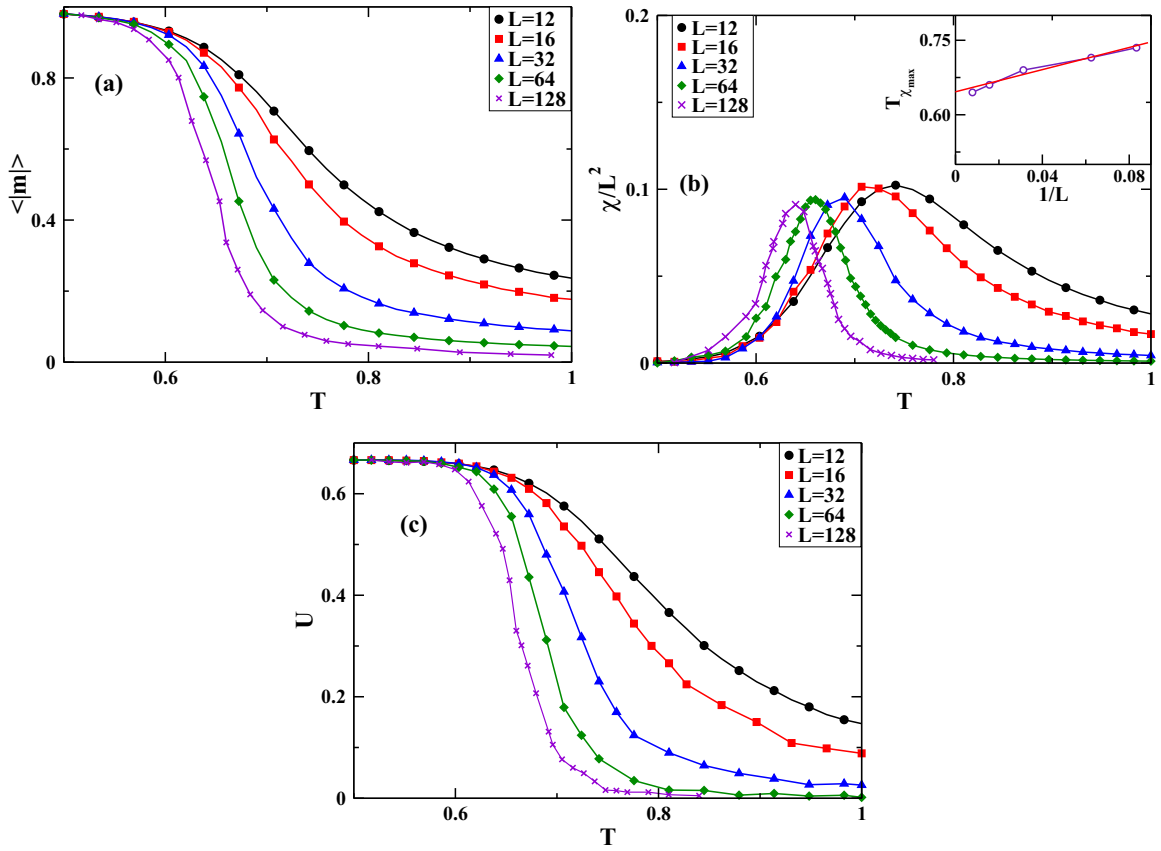

FIG. 6. (Color online) (a) Average absolute value of the magnetization, $\langle|m|\rangle$, (b) susceptibility, $k_B T\chi$, and (c) Binder cumulant, U, versus the temperature, obtained for $D = 0$ and samples of different size, as indicated. The inset in (b) shows the extrapolation of the finite-size effective critical temperatures corresponding to the peaks of χ ($T_{\chi_{\max}}$ versus $L^{-1/\nu}$ with $\nu = 1$), which yields $k_B T_c/J = 0.647(15)$ in the $L \to \infty$ limit.

D is large and impurities dominate, generating isolated islands of spins on the sample. The number of these islands increases with the size and it is necessary to increase the temperature to observe a paramagnetic phase. The competition between those two different behaviors that occurs close to the tricritical point, where both first- and second-order transitions meet, may be the reason of the absence of sample size effects in the location of the tricritical point. Although there may be scaling corrections that cannot been observed within the limited size of the lattices considered in this work, our extensive

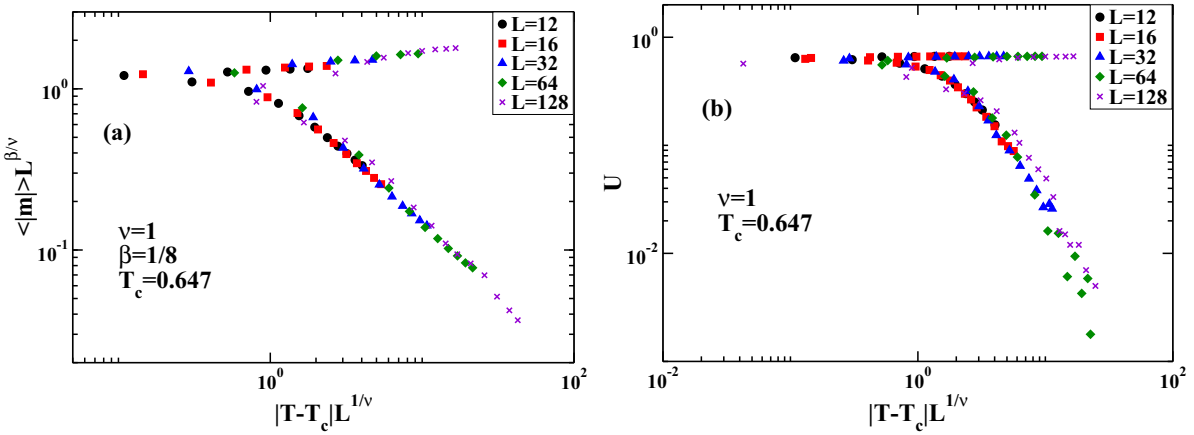

FIG. 7. (Color online) (a) Scaling plots of the average absolute value of the magnetization, $\langle|m|\rangle L^{\beta/\nu}$ versus $|T - T_c|L^{1/\nu}$, obtained by setting $\beta = 1/8$, $\nu = 1$, and the critical temperature $k_B T_c/J = 0.647$, following the best fit to the data shown in the inset to Fig. 6(b). (b) Scaling plots of the Binder cumulant. Both panels show data corresponding to $D = 0$ and obtained for lattices of different size, as indicated.

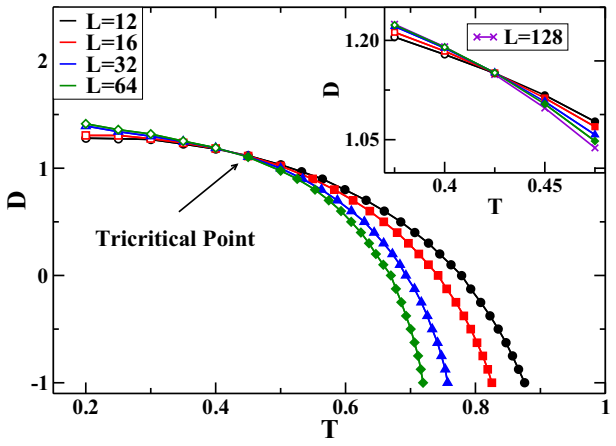

FIG. 8. (Color online) Phase diagram of the MEM-BC model obtained for samples of different linear size L, as indicated. Solid and open symbols indicate lines of second- and first-order effective transitions, respectively, which meet at the effective tricritical point. The inset displays a close-up view, which shows that the tricritical point is essentially independent of the sample size.

simulations indicate the existence of a true tricritical point located at ($k_B T_{\rm tri}/J = 0.425(10)$, $D_{\rm tri}/J = 1.145(10)$), where the error bars estimate both statistical errors and finite-size effects.

IV. CONCLUSIONS

Motivated by an interest to contribute to a deeper understanding of magnetic thin-film growth by deposition, which is widely used in the fabrication of MEMs, impurities were incorporated to a $(2+1)$-dimensional MEM model previously studied [42]. Since the quality and performance of magnetic devices are strongly determined by the purity, structural integrity, and degree of homogeneity of their epitaxial layers, impurities (or vacancies) produce a decrease in the interface magnetization, which is particularly undesired. In most experimental setups, thin films are grown far from thermodynamic equilibrium. In this work, we have presented a nonequilibrium model, which considers a three-state spin system ($s_i = \pm 1,0$) to study the influence of impurities in the growth of magnetic thin films with strip geometries. We have also compared our results with those from its equilibrium counterpart, namely the 2D Blume-Capel model.

The MEM-BC model's properties are dependent upon two parameters: the temperature (T) that controls thermal fluctuations and the crystal field (D) that governs the density of impurities. Despite its apparent simplicity, this model presents a rich variety of stationary states and different growth regimes that depend on the values of T and D. In the absence of impurities (or vacancies), previous studies have established that the model presents two phases, paramagnetic and ferromagnetic, separated by a continuous, second-order transition [42]. Here, we found analogous results for low enough concentrations of impurities, in which densities of spins and impurities show a smooth change with T and D when crossing the second-order transition. Besides these two phases, moreover, nonmagnetic, impurity-dominated states appear for large values of D and they change into ferromagnetic states across a first-order transition, by either decreasing the temperature, the crystal field, or both. Across this type of transition, the densities of impurities and spins change abruptly. We have established the type of transitions also studying the susceptibility and the Binder cumulant for the magnetization and the density of impurities, which show sharp or smooth behavior according to the transition being first or second order, respectively. Furthermore, using finite-size scaling analysis, we obtained critical exponents for the second-order transition, which, intriguingly, are the same as those corresponding to the 2D Blume-Capel model under equilibrium conditions. Finally, the first- and second-order transition lines were found to meet each other at a tricritical point located at $D_t/J = 1.145(10)$ and $k_B T_t/J = 0.425(10)$, which appears to be independent of the sample size within the accuracy of our simulations.

ACKNOWLEDGMENTS

This work was financially supported by CONICET, UNLP, and Agencia Nacional de Promoción Científica y Tecnológica de la República Argentina (Argentina).

[1] R. F. Bunshah, *Handbook of Deposition Technologies for Films and Coatings*, 2nd ed. (Noyes Publications, Westwood, 1994).
[2] J. E. Mahan, *Physical Vapor Deposition of Thin Films* (Wiley, New York, 2000).
[3] M. Ohring, *Materials Science of Thin Films: Deposition and Structure*, 2nd ed. (Academic Press, San Diego, 2002).
[4] D. A. Glocker, C. Morgan, and S. I. Shah, *Handbook of Thin Film Process Technology*, 2nd ed. (Taylor & Francis, London, 2010).
[5] *Multilayer Thin Films: Sequential Assembly of Nanocomposite Materials*, edited by G. Decker and J. B. Schlenoff (Wiley-VCH, Weinheim, 2002).
[6] *Nano-Architectured and Nano-Structured Materials*, edited by Y. Champion and H.-J. Fecht (Wiley-VCH, Weinheim, 2004).
[7] *Handbook of Nanostructured Thin Films and Coatings*, edited by S. Zhang (CRC Press, Boca Raton, 2010), Vol. 13.
[8] T. M. Squires and S. R. Quake, Rev. Mod. Phys. **77**, 977 (2005).
[9] K. M. Seemann, V. Baltz, M. MacKenzie, J. N. Chapman, B. J. Hickey, and C. H. Marrows, Phys. Rev. B **76**, 174435 (2007).
[10] J. S. Chen, J. F. Hu, B. C. Lim, W. L. Phyoe, B. Liu, and G. Ju, J. Appl. Phys. **105**, 07B724 (2009).
[11] B. Wang, D. C. Berry, Y. Chiari, and K. Barmak, J. Appl. Phys. **110**, 013903 (2011).
[12] R. Monnier and B. Delley, Phys. Rev. Lett. **87**, 157204 (2001).
[13] K. Maiti, V. R. R. Medicherla, S. Patil, and R. S. Singh, Phys. Rev. Lett. **99**, 266401 (2007).
[14] K. Maiti, Europhys. Lett. **82**, 67006 (2008).
[15] S. K. Pandey and R. J. Choudhary, J. Phys.: Condens. Matter **23**, 276005 (2011).

[16] S. B. Ogale, R. J. Choudhary, J. P. Buban, S. E. Lofland, S. R. Shinde, S. N. Kale, V. N. Kulkarni, J. Higgins, C. Lanci, J. R. Simpson, N. D. Browning, S. Das Sarma, H. D. Drew, R. L. Greene, and T. Venkatesan, Phys. Rev. Lett. **91**, 077205 (2003).
[17] S. R. Shinde, S. B. Ogale, J. S. Higgins, H. Zheng, A. J. Millis, V. N. Kulkarni, R. Ramesh, R. L. Greene, and T. Venkatesan, Phys. Rev. Lett. **92**, 166601 (2004).
[18] J. M. D. Coey, M. Venkatesan, and C. B. Fitzgerald, Nat. Mater. **4**, 173 (2005).
[19] A. J. Behan, A. Mokhtari, H. J. Blythe, D. Score, X.-H. Xu, J. R. Neal, A. M. Fox, and G. A. Gehring, Phys. Rev. Lett. **100**, 047206 (2008).
[20] J. T. Ji, A. M. Zhang, T. L. Xia, Q. Cao, G. L. Liu, D. Hou, and Q. M. Zhang, Phys. Rev. B **82**, 014408 (2010).
[21] M. Blume, Phys. Rev. **141**, 517 (1966); H. W. Capel, Physica **32**, 966 (1966).
[22] A. N. Berker and M. Wortis, Phys. Rev. B **14**, 4946 (1976); J. M. Yeomans and M. E. Fisher, *ibid.* **24**, 2825 (1981).
[23] M. J. Stephen and J. L. McCauley Jr., Phys. Lett. A **44**, 89 (1973); G. F. Tuthill, J. F. Nicoll, and H. E. Stanley, Phys. Rev. B **11**, 4579 (1975).
[24] D. P. Landau and R. H. Swendsen, Phys. Rev. Lett. **46**, 1437 (1981); Phys. Rev. B **33**, 7700 (1986).
[25] W. J. Camp and J. P. Van Dyke, Phys. Rev. B **11**, 2579 (1975); T. W. Burkhardt and R. H. Swendsen, *ibid.* **13**, 3071 (1976).
[26] P. D. Beale, Phys. Rev. B **33**, 1717 (1986).
[27] J. C. Xavier, F. C. Alcaraz, D. Penã Lara, and J. A. Plascak, Phys. Rev. B **57**, 11575 (1998).
[28] W. Selke, Surf. Sci. **144**, 176 (1984).
[29] A. Zaim, Y. El Amraoui, M. Krouad, and H. Arhchoui, J. Magn. Magn. Mater. **320**, 1030 (2008).
[30] R. da Silva, N. A. Alves, and J. R. Drugowich de Felício, Phys. Rev. E **66**, 026130 (2002); B. C. S. Grandi and W. Figueiredo, *ibid.* **70**, 056109 (2004).
[31] C. J. Silva, A. A. Caparica, and J. A. Plascak, Phys. Rev. E **73**, 036702 (2006).
[32] J. W. Tucker, J. Magn. Magn. Mater. **237**, 215 (2001); E. Albayrak and M. Keskin, *ibid.* **261**, 196 (2003).
[33] M. Keskin, O. Canko, and Ü. Temizer, Phys. Rev. E **72**, 036125 (2005).
[34] A. Malakis, A. N. Berker, I. A. Hadjiagapiou, and N. G. Fytas, Phys. Rev. E **79**, 011125 (2009).
[35] E. Albayrak, Physica A **390**, 1529 (2011); J. Magn. Magn. Mater. **323**, 2846 (2011).
[36] E. V. Albano and K. Binder, Phys. Rev. E **85**, 061601 (2012).
[37] E. V. Albano and K. Binder, Phys. Rev. Lett. **109**, 036101 (2012).
[38] T. Michely and J. Krug, *Islands, Mounds and Atoms Patterns and Processes in Crystal Growth Far from Equilibrium* (Springer, Berlin, 2004).
[39] J. W. Evans, P. A. Thielb, and M. C. Bartelt, Surf. Sci. Rep. **61**, 1 (2006).
[40] G. Antczak and G. Ehrlich, *Surface Diffusion Metals, Metal Atoms, and Clusters* (Cambridge University Press, Cambridge, 2010).
[41] M. Ausloos, N. Vandewalle, and R. Cloots, Europhys. Lett. **24**, 629 (1993); N. Vandewalle and M. Ausloos, Phys. Rev. E **50**, R635 (1994).
[42] J. Candia and E. V. Albano, Phys. Rev. E **63**, 066127 (2001); **84**, 050601(R) (2011).
[43] M. Eden, in *Symposium on Information Theory in Biology*, edited by H. P. Yockey (Pergamon Press, New York, 1958); in *Proceedings of the 4th Berkeley Symposium on Mathematics, Statistics and Probability*, edited by F. Neyman (University of California Press, Berkeley, 1961), Vol. IV, p. 223.
[44] K. Binder and D. W. Heermann, *Monte Carlo Simulations in Statistical Physics: An Introduction*, 4th ed. (Springer-Verlag, Berlin, 2002).
[45] K. Binder and D. Heermann, *A Guide to Monte Carlo Simulations in Statistical Physics* (Cambridge University Press, Cambridge, 2000).
[46] A. Achahbar, P. L. Garrido, J. Marro, and M. A. Muñoz, Phys. Rev. Lett. **87**, 195702 (2001).
[47] E. V. Albano, Phys. Rev. B **42**, 10818 (1990).
[48] S. Sarbach and I. D. Lawrie, in *Phase Transitions and Critical Phenomena*, edited by C. Domb and J. L. Lebowitz (Academic Press, London, 1984), Vol. 9, p. 1.
[49] G. Grinstein, C. Jayaprakash, and Y. He, Phys. Rev. Lett. **55**, 2527 (1985).
[50] B. Drossel and M. Kardar, Phys. Rev. E **55**, 5026 (1997).